https://doi.org/10.5194/wcd-2022-23
Preprint. Discussion started: 19 April 2022


Weather and Climate Dynamics Discussions
Open Access
EGU

# Signatures of midlatitude heat waves in global Rossby wave spectra

Iana Strigunova, Richard Blender, Frank Lunkeit, and Nedjeljka Žagar

Meteorological Institute, Center for Earth System Research and Sustainability (CEN), Universität of Hamburg, Grindelberg 5, 20144 Hamburg, Germany

**Correspondence:** Iana Strigunova (iana.strigunova@uni-hamburg.de)

**Abstract.** The paper investigates systematic changes of the global atmospheric circulation during midlatitude heat waves. The global balanced circulation is defined in terms of the Rossby wave solutions of the linearized primitive equations. The circulation variability is assessed by the probability density functions (PDFs) of the normalized total energy anomalies with respect to their climatological values. The evaluation is performed in wavenumber space defined by the zonal wavenumbers, meridional modes and vertical structure functions. Heat waves are defined by spatially averaged surface temperatures in Eurasia (bounded by the Ural) above the 95% percentile on at least three consecutive days. Normalized energy anomalies of the Rossby waves are found to be $\chi^2$-distributed with a skewness associated with the number of degrees of freedom. The PDFs of energy anomalies during heat waves are compared with their climatological distributions for the zonal mean flow, for the planetary and for the synoptic scales. During heat waves, the skewness of PDFs of planetary-scale circulation is increased up to a factor of two. The increase is associated with a drastic reduction of the number of degrees of freedom down to $1/4$ compared to climatology. This reduction explains the coarse structure of blocking events in the midlatitude troposphere as confirmed by the reconstructed circulation in physical space. The changes in variability are also assessed by investigating submonthly circulation variance across scales. Planetary waves are found to be more persistent during heat waves, while the synoptic waves vary more, which is consistent with the idea of circulation blocking during the extreme heat events. The presented diagnostics can be applied for other extreme events in the atmosphere.

Keywords: heat waves, Rossby waves, variability changes, global energy distribution, skewness

## 1 Introduction

The enhancement of planetary and synoptic-scale Rossby waves has been linked to the occurrence or formation of heat waves in mid-latitudes. However, the relation between anomalies in global Rossby circulation and heat waves remains unclear. Moreover, there is no robust method allowing us to identify signatures of heat waves in the global atmospheric spectrum. As a possible way to determine signatures common not only for case studies of heat waves but for their composite, statistical analysis can be a suitable tool. Statistical properties of mid-latitude circulation during extreme events were examined by recent studies (Screen and Simmonds, 2014; Coumou et al., 2014; Kornhuber et al., 2019). They have identified significant anomalies in the

https://doi.org/10.5194/wcd-2022-23
Preprint. Discussion started: 19 April 2022


Weather and Climate Dynamics Discussions
Open Access
EGU

planetary- and synoptic-scale Rossby waves by using the Fourier amplitudes and phases of temperature and wind variables. Namely, Screen and Simmonds (2014) have found a significant increase in the monthly variance and mean of anomalies of the Fourier amplitudes of 500 hPa geopotential heights for zonal wavenumbers 3-8 and suggested that amplified planetary waves are connected with temperature and precipitation extremes. Coumou et al. (2014) have analyzed wind fields at 300 and 500 hPa and found out that zonal wavenumbers 6-8 are the most probable candidates for quasi-resonance conditions according to Petoukhov et al. (2013). More recently, Kornhuber et al. (2019) have shown the coupling between the wavenumber 7 in daily wind and temperature data on several vertical levels (850, 700, 500, 300 hPa) and surface extreme events, such as heat waves and floods which occurred during the boreal summer 2018. The drawback of the one-dimensional Fourier method, performed along the latitude circles, is its lack of coupling between mass and velocity fields. We suggest the NMF decomposition as more rigorous compared to the Fourier approach because the NMF is a multivariate decomposition that represents simultaneously the velocity and mass fields using the Hough harmonics.

The NMF decomposition projects three-dimensional (3D) geopotential and wind data on the Rossby and inertia-gravity waves, which are eigensolutions of the linearized primitive equations on the sphere (Žagar and Tribbia, 2020). We use reanalysis data decomposed using this approach to analyse whether and how surface heat waves in Eurasia affect the global atmospheric variability spectrum. Therefore, we aim at answering the following question: how do heat extremes appear in the global atmospheric variability spectrum? While it is not evident a priori that surface heat waves during boreal summer have their fingerprints in the whole atmosphere Rossby wave spectra, we show that this is, in fact, the case. We carry out statistical analysis on the time series of the Hough expansion coefficients of the 3D reanalysis data similar to Žagar et al. (2020) and references therein. This statistical analysis allows us, for the first time, to estimate the distribution of the global Rossby circulation and its total energy.

The distribution of atmospheric fields are in general shown to be non-Gaussian (Sura et al., 2005; Perron and Sura, 2013). However, the Central Limit Theorem may still be applicable when the sums of components in high-dimensional systems are involved, with assumptions of independent and identical distributions of summing components. Under the independence of component or variable in a high-dimensional system, we consider that its time series are uncorrelated. The identity of distributions of summing components can be regarded in terms of their mean and variances being equal. In our analysis, it is not strictly necessary that the Hough coefficients are independent and identically Gaussian distributed since we assess changes in the energy distributions. These changes are diagnosed considering the skewness of the distributions. Even in the interpretation of the number of active degrees of freedom, we consider changes and not absolute values. Thus, the assumption of independent Gaussian distributed coefficients is not essential for interpreting the results. Nevertheless, we find that the Gaussianity of the coefficients and the corresponding $\chi^2$-distribution of the energy in individual modes are satisfied to a high degree.

The skewness, $\gamma$, of the $\chi^2$-distribution is given by $\sqrt{8/df}$ and the excess kurtosis, $\kappa$, is given by $12/df$ with the number of independent degrees of freedom, $df$ (Wilks, 2011). Because the atmospheric circulation is the composite of the zonal mean state and the superposition of waves (or the sum of multiple modes because of orthogonality of 3D eigenfunctions) which might be dependent, the statistical properties might deviate from the ideal situation. Further, we demonstrate that the distributions of

https://doi.org/10.5194/wcd-2022-23
Preprint. Discussion started: 19 April 2022


Weather and Climate Dynamics Discussions
Open Access
EGU

the energy anomalies can appear visually close to the Normal distribution due to the Central Limit Theorem for large degrees of freedom. However, the energy anomalies distributions are still skewed, which can be considered as an inherited property from energy distributions. For this reason, we consider skewness as the primary measure to characterise the behaviour of the Rossby circulation during the heat waves.

The paper is organized as follows. The data decomposition method, statistical analysis and the heat waves identification algorithm are explained in Section 2. In Section 2.3 we describe the data used for NMF decomposition and identification algorithm. In Section 3 we present examples of decomposition for two recent heat waves, the results of statistical analysis (climatology and during heat waves) and further interpretation by filtering part of Rossby circulation back to physical space. In the last chapter of Section 3, we discuss how temporal variance spectra changes during heat waves. In Section 4 we present final remarks.

## 2 Method and Data

### 2.1 Normal-mode function decomposition

Three-dimensional wind and geopotential fields are projected on NMFs in modal space. NMFs consist of vertical and horizontal structure functions (VSFs and HSFs, respectively). VSFs are the numerical solutions of the vertical structure equation and HSFs are given in terms of the Hough harmonics. The projection is performed in two steps (Žagar et al., 2015). In the first step, the data $\mathbf{X}(\lambda,\phi,\sigma)$ with longitude ($\lambda$), latitude ($\phi$), vertical level ($\sigma$) and at time $t$, is expanded into a series of orthogonal vertical structure functions $G_m$ according to

$$\mathbf{X}(\lambda,\phi,\sigma) = (u,v,h)^T = \sum_{m=1}^{M} \mathbf{S}_m \mathbf{X}_m(\lambda,\phi) G_m(\sigma). \tag{1}$$

The vertical mode index ($m$) ranges from 1 (known as the external mode) to $M$, the total number of vertical modes. For every $m$, the vector $\mathbf{X}_m(\lambda,\phi) = (\tilde{u},\tilde{v},\tilde{h})^T$ is normalized by the scaling 3×3 diagonal matrix $\mathbf{S}_m$ with elements $\sqrt{gD_m}$, $\sqrt{gD_m}$, $D_m$ where $D_m$ is equivalent depth.

The first seven vertical structure functions (VSFs) are presented in Fig. 1. The external mode ($m = 1$) and the subsequent four other modes ($m = 2-5$) do not change sign below the tropopause, and are regarded as troposphere-barotropic modes.

In the second step, for every $m$, the horizontal nondimensional motions are projected onto a series of Hough harmonics $\mathbf{H}_n^k$ with the complex Hough expansion coefficients $\chi_n^k(m)$,

$$\mathbf{X}_m(\lambda,\phi) = \sum_{n=1}^{R} \sum_{k=-K}^{K} \chi_n^k(m) \mathbf{H}_n^k(\lambda,\phi;m), \tag{2}$$

where $K$ denotes the total number of zonal waves, $R$ denotes the total number of meridional modes which contains three motions in the atmosphere: Rossby modes, eastward and westward inertia-gravity modes.

The horizontal structure functions (HSFs) are given in terms of the Hough harmonics $\mathbf{H}_n^k$ which are defined as

$$\mathbf{H}_n^k(\lambda,\phi,m) = \Theta_n^k(\phi,m) e^{ik\lambda}, \tag{3}$$

https://doi.org/10.5194/wcd-2022-23
Preprint. Discussion started: 19 April 2022


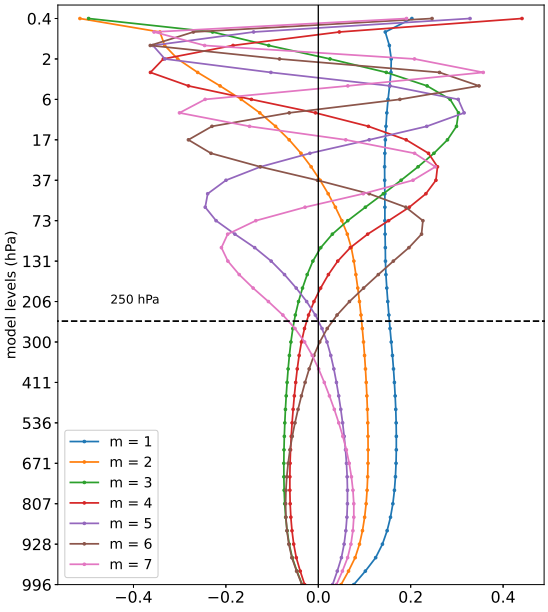


**Figure 1.** Vertical structure functions (VSFs) for the first seven vertical modes derived using 43 model levels in ERA-Interim. Modes that do not cross zero below the tropopause (here we refer to 250 hPa level) are regarded as barotropic tropospheric modes.

with the meridional Hough vector function $\Theta_n^k = [U_n^k(\phi,m), iV_n^k(\phi,m), Z_n^k(\phi,m)]^T$, harmonic waves $e^{ik\lambda}$ in the longitudinal direction with the zonal wavenumber $k$, and the meridional mode index $n$ for every $m$.

Hence, the Hough expansion coefficient, $\chi_n^k(m)$, is obtained as

$$\chi_n^k(m) = \frac{1}{2\pi}\int_0^{2\pi}\int_{-1}^{1} \mathbf{X}_m(\lambda,\phi)[\mathbf{H}_n^k]^* d\mu d\lambda. \tag{4}$$

### 2.2 Total energy of balanced atmospheric circulation

The first step in the statistical analysis of the Rossby modes (the balanced circulation) considers the probability distribution of the real and imaginary parts of the Hough coefficients. We find that real and imaginary parts are Gaussian distributed for a single Rossby mode in the synoptic wavenumber range. Since in physical space kinetic energy is the sum of the squares of the horizontal wind components, the distributions of the energy components are approximately $\chi^2$-distributed with a distinct non-zero skewness. We do not normalise the coefficients in single modes to unity variance for the purpose of retaining the different energy contributions. Thus we do not consider energy distributions as exactly $\chi^2$-distributed, but we will assess changes of the skewness during heat waves as an indicator for the changes in the atmospheric circulation. The total energy is given in terms

https://doi.org/10.5194/wcd-2022-23
Preprint. Discussion started: 19 April 2022


of the real and imaginary parts of the Hough coefficients

$$I_n^k(m) = \frac{1}{2} g D_m |\chi_n^k(m)|^2 = \frac{1}{2} g D_m [(\mathrm{Re}\chi_n^k(m))^2 + (\mathrm{Im}\chi_n^k(m))^2], \tag{5}$$

where $g$ is the gravitational acceleration and $D_m$ are the equivalent depths.

We consider the extended boreal summer (MJJAS, May-September) during which the major part of heat waves in the mid-latitudes occur.

The energy computed from the daily Hough coefficients is $I_{d,y}$ with $d$ denoting the day in MJJAS and $y$ denoting the year in the datasets. We calculate the climatological mean of the annual cycle

$$\langle I_{d,y} \rangle_y = \frac{1}{N_y} \sum_{y=1}^{N_y} I_{d,y}, \tag{6}$$

for each day in MJJAS (153 in total).

The energy deviations (or anomalies) from the climatological annual cycle $\langle I_{d,y} \rangle_y$ are

$$I' = I - \langle I \rangle_y, \tag{7}$$

where $I$ denotes $I_{d,y}$ for brevity. At this stage, we form new time series of energy anomalies with time steps of the observed heat waves (Table 1). Then, we compute normalized energy anomalies by

$$\tilde{I'} = \frac{I'(t)}{\sigma} \tag{8}$$

with their climatological standard deviation $\sigma$. Note that the entire time series of energy anomalies (climatology) and time series only during heat waves are normalized by different $\sigma$.

This procedure is applied mode-wise for every dataset independently. The next step is to split the normalized energy anomalies of the single Rossby modes into planetary ($k = 1, 2, 3$) and synoptic ($k = 4 - 10$) intervals, and then to average only the troposphere-barotropic modes $m = 1 - 5$ within these intervals. The zonal flow is given by $k = 0$. In each case, all meridional modes are averaged except for the first one, which corresponds to the mixed Rossby-gravity mode and is counted among the balanced modes in MODES software.

Lastly, we combine all reanalyses in the above-mentioned atmospheric flows. Žagar et al. (2020) showed that the differences between climatological energy spectra for the four reanalyses are minor. Therefore, our PDFs consist of independent but similar time series. Thus, we can detect robust features of distributions of energy anomalies across different datasets.

### 2.3 Data

To reduce statistical uncertainty, we project four reanalyses: ERA5 (Hersbach et al., 2020), Era-Interim (Dee et al., 2011), the Japanese 55-year Reanalysis JRA-55 (Kobayashi et al., 2015), and the Modern-Era Retrospective analysis for Research and Applications MERRA (Rienecker et al., 2011). We use daily data at 12:00 UTC from 1980-2014 (1980-2019 for ERA5) on $256 \times 128$ grid points in the zonal and meridional directions, respectively. We interpolate this data on the predefined 43 $\sigma$

https://doi.org/10.5194/wcd-2022-23
Preprint. Discussion started: 19 April 2022




levels. After the NMFs projection to modal space, we obtain the daily time series of Hough coefficients with the following truncations: $K = 101, M = 27, R = 150$, where $M$ denotes the number of vertical modes and $K$ includes the zonal mean flow ($k = 0$). $R$ combines equal numbers of meridional modes ($n = 50$) for the Rossby modes, eastward inertia-gravity modes and westward inertia-gravity waves modes.

We analyse heat waves for the Eurasian region limited by the Ural mountains $[35°N - 65°N, 10°W - 60°E]$. The choice of the study area is defined by capturing the most significant atmospheric processes occurring during heat waves. For heat wave identification, we analyse daily 2 m temperature fields for the extended boreal summer (MJJAS) from 1980-2014 (until 2019 for ERA5). The identification algorithm applied by Ma and Franzke (2021) uses the following two criteria: (i) the temperature exceeds the 95th percentile threshold and (ii) the duration of the exceedance is larger than three consecutive time steps. As the identification algorithm is performed for each reanalysis, it is expected to have discrepancies among them. Therefore, we form a list of heat waves as a list of physically consistent extreme events. We find that the total number of days with heat waves affects the statistical significance of results in modal space. When the results of the identification algorithm are more precise within the list of heat waves, the results of the statistical analysis in modal space are less significant due to the small sample size. Table 1 presents the list of days with heat waves, which is formed on the basis of the preconditions mentioned above.

## 3 Results

First, we confirm that the global energy in a single Rossby mode is $\chi^2$-distributed using the climatology from 1980-2014. In our example, we use the energy (Eq. 5) of the balanced mode with $k = 7$, $n = 3$ associated with a significant part of mid-latitude circulation, and $m = 1$. The histogram and the fit of the $\chi^2$-distribution with two degrees of freedom, $df = 2$, corresponding to the real and the imaginary parts is shown in Fig. 2. The Kolmogorov-Smirnov test reveals a negligible $p$-value, confirming the fit. Therefore, we find that approximation of $\chi^2$-distributed energy is satisfied to a high degree.

https://doi.org/10.5194/wcd-2022-23
Preprint. Discussion started: 19 April 2022


Weather and Climate Dynamics Discussions
Open Access
EGU

**Table 1.** Heat waves in Eurasia during May-September 1980-2019

| | | ERA5 | ERA-Interim | JRA-55 | MERRA |
|---|---|---|---|---|---|
| | Start date | Number of detected days | | | |
| 1 | 1994-09-23 | 3 | 3 | 2 | 3 |
| 2 | 2006-06-18 | 12 | 10 | 12 | 10 |
| 3 | 2006-09-20 | 3 | 5 | 6 | 2 |
| 4 | 2007-05-20 | 12 | 12 | 12 | 12 |
| 5 | 2007-08-21 | 6 | 6 | 6 | 6 |
| 6 | 2008-09-05 | 4 | 3 | 4 | 3 |
| 7 | 2010-06-28 | 26 | 27 | 27 | 26 |
| 8 | 2010-07-27 | 21 | 21 | 19 | 21 |
| 9 | 2012-05-09 | 4 | 4 | 4 | 4 |
| 10 | 2012-06-14 | 4 | 3 | 4 | 3 |
| 11 | 2013-05-02 | 7 | 7 | 6 | 5 |
| 12 | 2014-05-17 | 5 | 3 | 3 | 3 |
| 13 | 2014-06-05 | 5 | 6 | 5 | 6 |
| 14 | 2015-06-02 | 3 | - | - | - |
| 15 | 2015-08-11 | 3 | - | - | - |
| 16 | 2015-09-17 | 11 | - | - | - |
| 17 | 2016-06-21 | 4 | - | - | - |
| 18 | 2016-08-20 | 9 | - | - | - |
| 19 | 2018-05-02 | 8 | - | - | - |
| 20 | 2018-06-27 | 4 | - | - | - |
| 21 | 2018-07-13 | 22 | - | - | - |
| 22 | 2018-08-29 | 7 | - | - | - |
| 23 | 2018-09-11 | 12 | - | - | - |
| 24 | 2019-06-01 | 3 | - | - | - |
| 25 | 2019-06-08 | 5 | - | - | - |
| 26 | 2019-06-18 | 3 | - | - | - |
| 27 | 2019-06-23 | 4 | - | - | - |
| 28 | 2019-07-24 | 3 | - | - | - |
| ∑N. of days | | 213 | 110 | 110 | 104 |

https://doi.org/10.5194/wcd-2022-23
Preprint. Discussion started: 19 April 2022


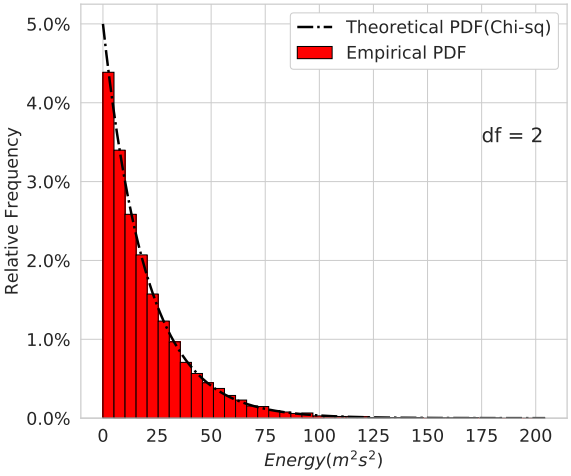


**Figure 2.** Atmospheric energy (empirical) distribution in the Rossby (balanced) regime with zonal wavenumber ($k = 7$), meridional mode ($n = 3$) and vertical index ($m = 1$) for 1980-2014. The dashed black lines correspond to the theoretical ($\chi^2$) distribution ($df$ are the degrees of freedom).

### 3.1 Northern Hemisphere extratropical circulation decomposition

We present the decomposition of the climatological Rossby circulation and case studies for selected heat wave events. Here, we show only ERA5 results because other datasets demonstrate similar results. Figure 3a depicts the May-September balanced circulation (Rossby modes with $k > 0$ and all $m$) at a single $\sigma$-level close to 500 hPa. The pattern remains almost the same when we restrict vertical modes to only the troposphere-barotropic modes, $m = 1 - 5$ (Fig. 3b). Thus our selection of modes is suitable for the purpose of analysing the troposphere-barotropic circulation, i.e. the pattern observed during surface extreme events and often referred to as "atmospheric blocking". This structure is clearly recognized when we reconstruct circulation during two recent extreme heat events: the Russian Heat Wave in 2010 (Barriopedro et al., 2011) and the European Heat Wave in 2019 (Xu et al., 2020). The difference with respect to climatology which is presented in Fig. 3b. In both cases, we observe strong positive anomalies over the locations of the observed surface extremes (Western Russia and Europe) with nearby negative anomalies. For the Russian Heat Wave in Fig. 3c, d, the anomalies over Central and Southern Asia reveal cyclones which have produced extreme rainfall known as the Pakistan Flood (Lau and Kim, 2012). Furthermore, the wavy pattern along the latitudinal belt depicts teleconnections (Teng and Branstator, 2019). The plots with the difference between climatology and each heat wave (Fig. 3d, f) demonstrate the meridional extension of the waves from polar to tropical regions confirming the impact of these regions on mid-latitude extremes (Behera et al., 2012).

https://doi.org/10.5194/wcd-2022-23
Preprint. Discussion started: 19 April 2022


Weather and Climate Dynamics Discussions
Open Access
EGU

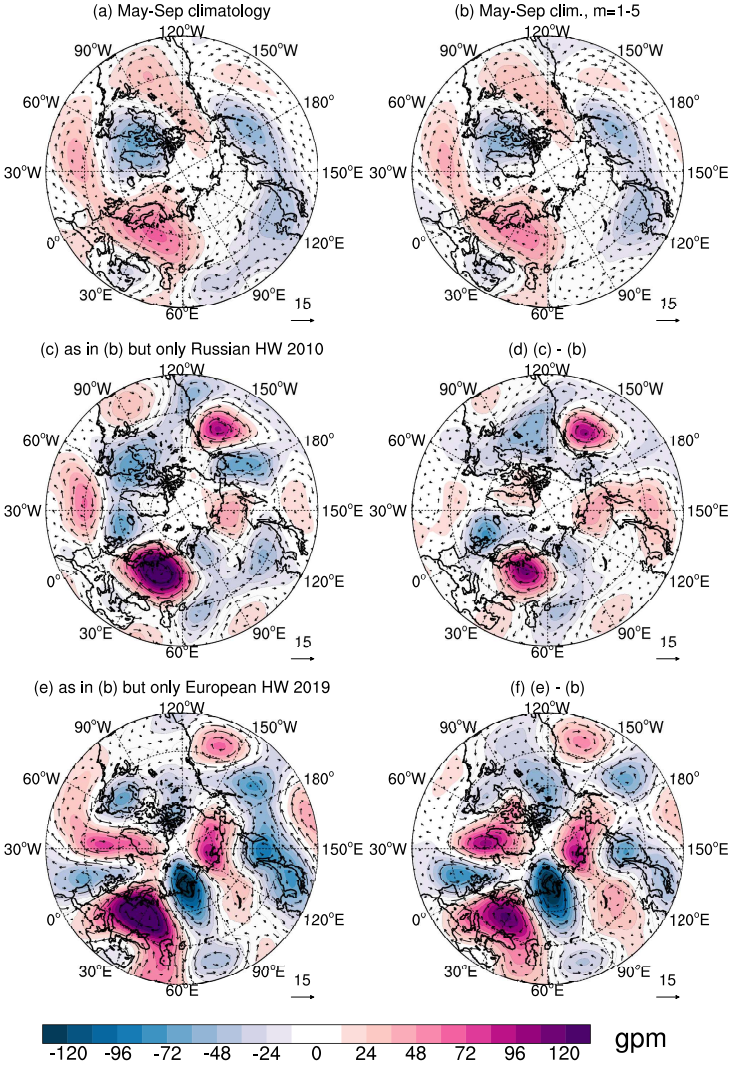


**Figure 3.** Climatological balanced circulation (Rossby modes for $k > 0$) for extended boreal summer at a terrain-following $\sigma$ level close to 500 hPa (ERA5 model level 30) in the mid-latitudes ($35^\circ N - 65^\circ N$). Coloured contours are geopotential height anomalies (gpm) for Rossby modes (a) including all zonal wavenumbers, meridional modes and vertical structure functions. The zonal mean state ($k = 0$) is not included. (b) as in (a) but only troposphere-barotropic vertical modes are included ($m = 1 - 5$), (c) as in (b) but for the Russian Heat Wave (HW) in 2010. (d) Difference between the (c) and (b). As in (c), (e, f) illustrate Rossby circulation during European Heat Wave (HW) 2019. Wind speed is shown by the length of the wind vectors (15 $\mathrm{ms}^{-}1$ as a reference vector).

https://doi.org/10.5194/wcd-2022-23
Preprint. Discussion started: 19 April 2022


Weather and Climate Dynamics Discussions
Open Access
EGU

### 3.2 Statistics in modal space

The decomposition in the previous section demonstrated how the Rossby circulation modified during heat waves. Our next step is to understand what the heat waves signatures in the global variability spectrum are and, therefore, their impact on global atmospheric circulation. Under the global variability spectrum, we imply the PDFs of the global energy anomalies and under signatures of heat waves, we imply significant changes in the distributions of energy anomalies. As a first step, we analyse the climatological PDFs of the normalized energy anomalies of modes with zonal wavenumbers corresponding to three intervals as described in Section 2 with emphasis on the skewness: (i) the zonal mean state, $k = 0$, (ii) the planetary-scale circulation $k = 1 - 3$, and (iii) the synoptic-scale circulation with $k = 4 - 10$. Figure 4a shows the PDF of the total Rossby circulation which clearly deviates from a Gaussian distribution. The PDFs of the planetary-scale (Fig. 4c) and the synoptic-scale (Fig. 4d) Rossby waves also do not follow a normal distribution, but exhibit noticeable asymmetry.

To determine this asymmetry, we consider the skewness of the PDFs for examined flows and all four reanalyses (ERA5, ERA-I, JRA-55, MERRA) combined. For a more robust statistical analysis, we apply bootstrapping with a replacement which results in an agreement between considered datasets - all values are within the defined 95% confidence intervals (CI) presented as horizontal lines at the ends of bars (Fig. 5a). The bootstrapped skewness shows that the normalized energy anomaly distribution has the highest asymmetry in the planetary scales and zonal mean circulation which is also detected as stretched right tails in the PDF. The different skewnesses in the four wavenumber ranges can partly be explained by varying degrees of freedom. For the latter, we refer to the number of single modes within the mentioned wavenumber ranges. However, changes in the dynamics can modify the skewness and the active degrees of freedom, and this is addressed in the next section.

#### 3.2.1 Surface extremes and energy statistics

As a second step, we calculated the energy anomalies during observed heat waves over Eurasia (28 events in total, see the methods section) and compare it with climatology for different parts of wavenumber space. For comparison, we consider two statistical moments, skewness and excess kurtosis, to diagnose the changes in shape, especially in the tails of distributions for the four reanalyses datasets. We find that only the difference in the skewness of the planetary-scale distribution is statistically significant, i.e the bootstrapped values are outside CIs of climatological bootstrapped skewness only during extremes.

The PDFs of the normalized energy anomalies depicted in Fig. 6 demonstrate how probabilities of the energy deviations change during surface extreme events. First, there is a positive shift in the mean except for $k = 0$, and, as a consequence, an increased probability of intermediate positive deviations. According to Fig. 5a, the change in the skewness, which is considered as the main indicator, is the largest for the planetary-scale circulation. The excess kurtosis for extreme events is approximately twice larger than climatology (Fig. 5b), which reflects a drastic rise in the probability of extreme values. The opposite change is found for the zonal mean flow during surface heat waves, where skewness and the excess kurtosis decrease; this implies that the distribution becomes flatter with thinner tails and is less extreme. Based on this, we conclude that the amplitudes of the planetary circulation amplify as shown in Fig. 3d, f, while the zonal mean flow anomalies become weaker in agreement with

https://doi.org/10.5194/wcd-2022-23
Preprint. Discussion started: 19 April 2022


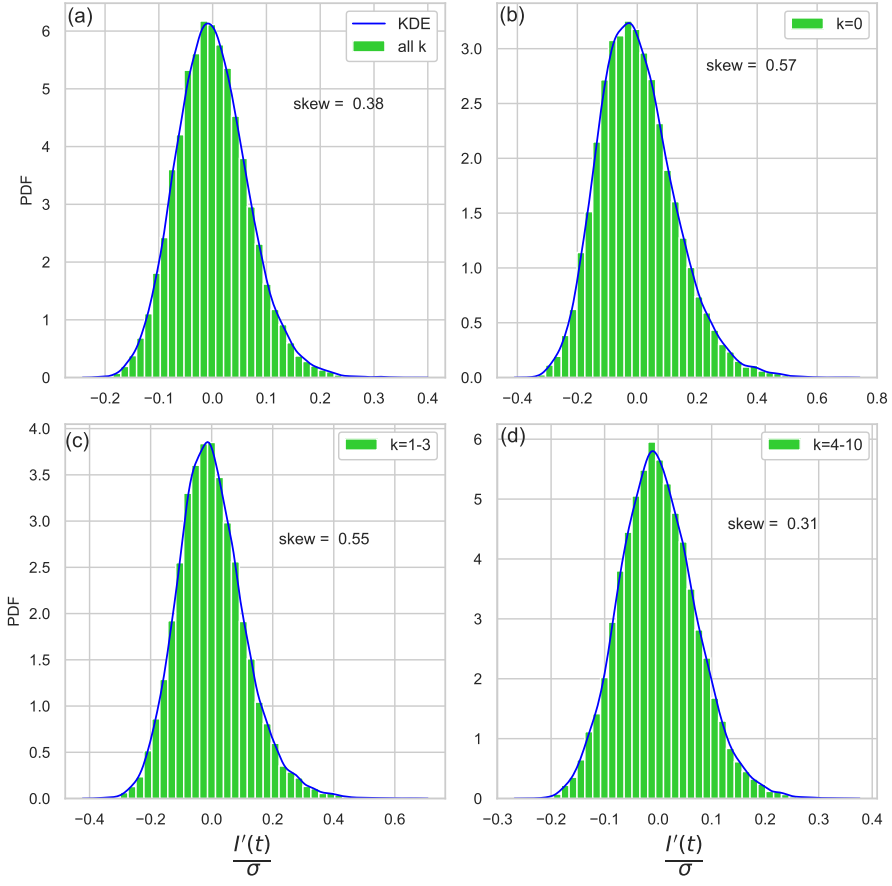


**Figure 4.** PDFs of normalized total energy anomalies (all $k$), (b) the zonal mean state ($k = 0$), (c) planetary-scale waves ($k = 1 - 3$), (d) synoptic-scale waves ($k = 4 - 10$). Empirical PDFs are depicted as green bars for extended boreal summer (MJJAS) 1980-2014 (1980-2019 for ERA5). The blue curve is the Kernel Density Estimator (KDE).

Coumou et al. (2015). Thus, we have evidence that signatures of heat waves are seen in different parts of the global variability spectrum via statistically significant changes in skewness.

The increase in skewness allows for the estimation of the reduction of the active dynamical degrees of freedom during the heat waves compared to the climatological mean. For the estimation, we use the exact relation for the skewness of $\chi^2$-distributed variable, $\gamma = \sqrt{8/df}$, with sums of $df$ as squares of the independent Gaussian variables with unit variance. We are not able to derive the absolute values in our analysis since this would require identifying the independent degrees of freedom in the set of modes, which is beyond the aim of the present study. (An estimation of absolute numbers of degrees of freedom using the $\chi^2$-distribution in geopotential height fields was presented in Fraedrich et al. (1995).)

However, we can derive the ratio $df_e/df_c = \gamma_c^2/\gamma_e^2$, where $df_e$ is the number of degrees of freedom during extreme events and $df_c$ is the number of degrees of freedom in climatology with the skewness $\gamma_e$ during extremes and the climatological mean

https://doi.org/10.5194/wcd-2022-23
Preprint. Discussion started: 19 April 2022


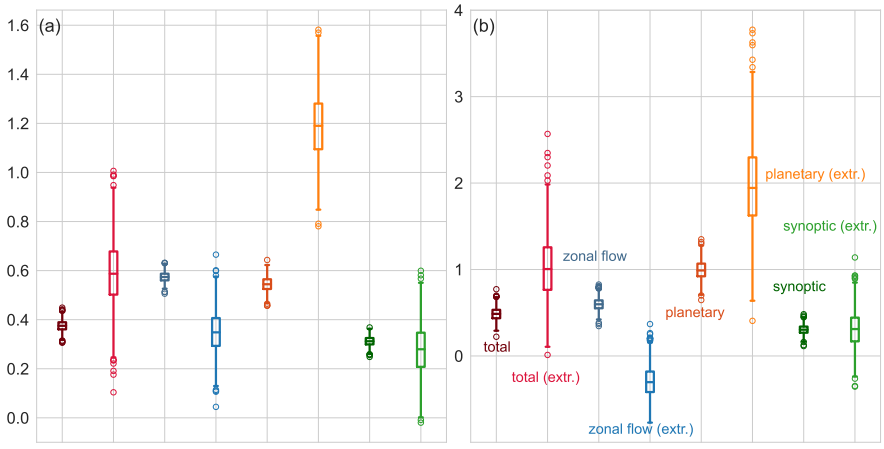


**Figure 5.** Box-plots for (a) skewness and (b) excess kurtosis of normalized energy anomalies distributions for four considered atmospheric components: total Rossby regime with dark- and light-red bars, the zonal mean flow as dark- and light-blue bars, planetary waves as orange and yellow, and the synoptic circulation as dark- and light-green 95%-confidence intervals are obtained through bootstrapping with replacement with 1000 simulations.

$\gamma_c$. The rough estimates $\gamma_e \approx 1.2$ and $\gamma_c \approx 0.6$, based on Fig. 5a, yield a reduction of the degrees of freedom of the order of $df_e/df_c \approx 1/4$ during the extreme events.

Since the projection in modal space is global, it is worthwhile to separate the entire atmosphere into symmetric and asymmetric components. The symmetry is defined with respect to the equator for the geopotential height and zonal wind fields. By considering symmetric and asymmetric modes, we find that both parts contribute to changes in the energy anomalies distribution. This means that Rossby waves in the Southern Hemisphere might have contributed to the results presented here for the Northern Hemisphere heat waves. Taking into account the lower frequency of atmospheric blocking (symmetric part) (Wiedenmann et al., 2002) in the Southern Hemisphere, we may assume that this influence is negligible. We also find that the Southern Hemisphere cyclones (asymmetric part) do not show significant change during the Northern Hemisphere heat waves.

### 3.3 Changes in the extratropical circulation during the heat waves

The next step is to relate the results to anomalies in physical space. This is achieved by filtering the analyzed Rossby modes ($k = 1-3, m = 2-50, m = 1-5$) to physical space, similar to what has been done in Fig. 3. Instead of case studies, we demonstrate the Rossby circulation averaged over days with observed extremes. We show again the horizontal circulation at ERA5 $\sigma$-level near 500 $\mathrm{hPa}$ as representative for the troposphere-barotropic circulation. Figures 7b and c reveal an enhancement of positive height anomalies in the eastern part of the Baltic Sea and negative anomalies over the North Atlantic. Moreover, one can notice a north-westward shift of negative anomalies in the Asian part compared to climatology presented in Fig. 7a and the formation of positive anomalies over Chukotka and Alaska. According to Fig. 7c, the dominant patterns are zonal wavenumber 2 and 3. Figures 7d, e show the vertical profile for $54°N$ of the meridional wind speed and the geopotential height

https://doi.org/10.5194/wcd-2022-23
Preprint. Discussion started: 19 April 2022


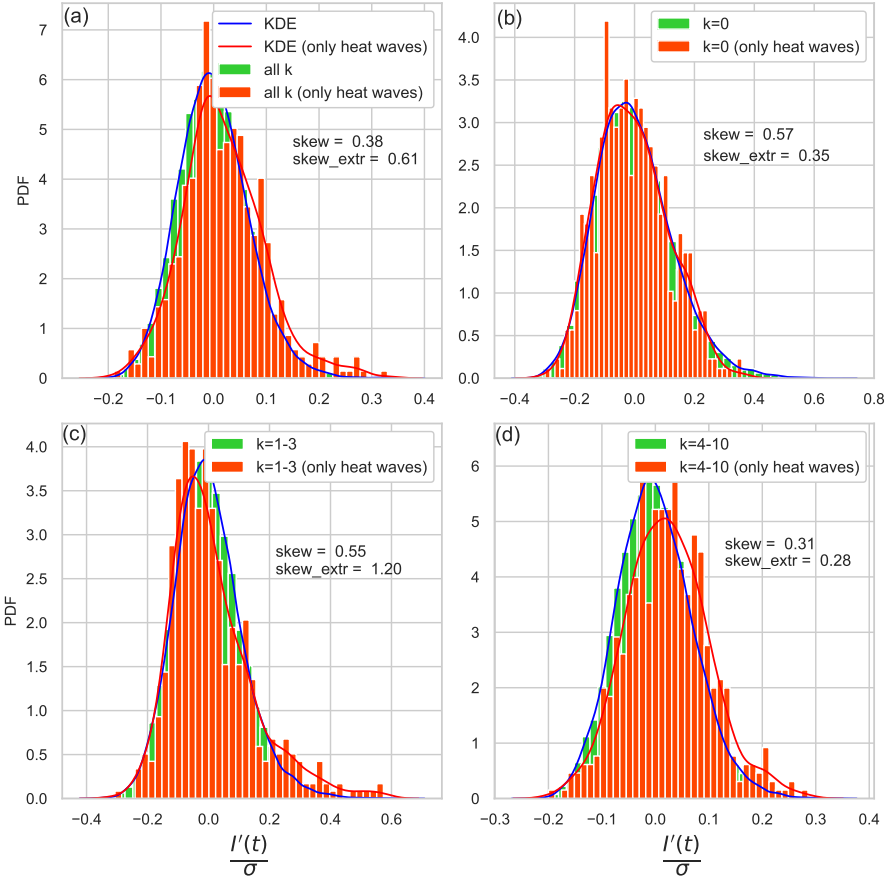


**Figure 6.** The same as in Fig. 4 but with normalized energy anomalies only during heat waves presented in Table 1.

anomalies for climatology, during heat waves. Figure 7f depicts the difference between two profiles. We illustrate again that the structure is barotropic over the entire troposphere and lower stratosphere, as was observed in some studies. Moreover, there is an enhancement of northward winds over Europe ($0°E-30°E$) and southward winds over the Asian part of Russia ($60°E-90°E$) with southerlies over the Kamchatka Peninsula (Fig. 7f). Overall, we find an increase in wave amplitudes, and change in phases as can be noticed by west- and northward shifts in Fig. 7b, c and Fig. 7d, e in the Baikal lake area ($90°E-120°E$). According to Teng and Branstator (2012) and Ragone and Bouchet (2021), the wave-3 pattern is dominant for heat waves that occurred in the US, France and Scandinavia. Therefore, the results agree with previous studies and demonstrate how surface extremes modify atmospheric circulation not only locally, but also in remote regions.

https://doi.org/10.5194/wcd-2022-23
Preprint. Discussion started: 19 April 2022


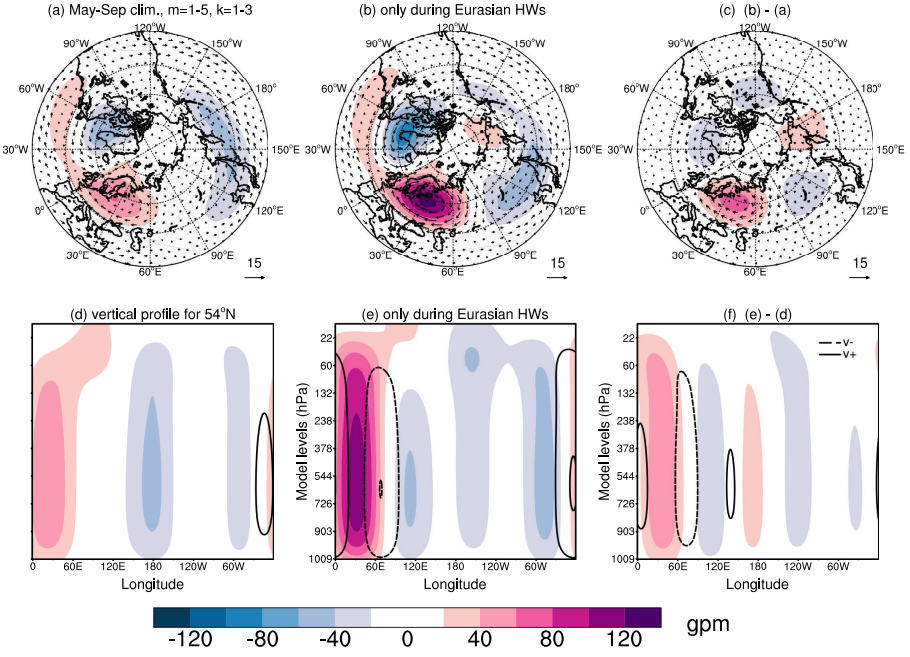


**Figure 7.** Atmospheric Rossby circulation filtered in physical space (only $k = 1-3, n = 2-50, m = 1-5$) at the $\sigma-$level close to 500 $\mathrm{hPa}$ in ERA5. Coloured contours are geopotential height anomalies, spaced by 20 $\mathrm{gpm}$, wind speed is shown by the arrow length. (a) Mean circulation in May-September obtained in the 40-year climatology (1980-2019), (b) composite of 28 Eurasian Heat Waves (HWs) presented in Table 1, (c) is the difference between (b) and (a). (d) Mean vertical profile at $54^{\circ}N$, (e) the same as (d) only during heat waves, (f) is the difference between (e) and (f). Solid and dashed contours illustrate the meridional wind (northward and southward, respectively) every 2 $\mathrm{ms}^{-1}$.

### 3.4 Heat waves in submonthly Rossby wave variance spectra

235 So far, we showed signatures of extremes in spatial variance. In contrast to the spatial variance (energy) spectra, temporal variance spectra are not well studied. Žagar et al. (2020) analyzed subseasonal variance and showed its statistically significant trends in planetary and synoptic scales. Here, we carry out a similar analysis for submonthly scales. Unbiased submonthly

https://doi.org/10.5194/wcd-2022-23
Preprint. Discussion started: 19 April 2022


variance ($\mathrm{Jkg}^{-}1$) is computed as

$$V_\nu = \frac{1}{N-1}\sum_{t=1}^{N} gD_m|\chi_\nu(t) - \bar{\chi_\nu}|^2 \tag{9}$$

where $\bar{\chi_\nu}$ is the monthly mean and $N$ is the number of days in a single month. Zonal wavenumber variance spectra are obtained by summing over the vertical modes, $m = 1-5$, and all meridional indices, except the first one, as

$$V_k = (2-\delta_{k0})\sum_{n=2}^{50}\sum_{m=1}^{5} V_\nu \tag{10}$$

where $\delta_{k0} = 0$ for $k > 0$ and $\delta_{k0} = 1$ for $k = 0$. To obtain the mean state, we average computed variances over all months (May-September) and years (1980-2019) in ERA5. To consider only extremes, we select variances within months with observed heat waves and then average for every mode separately. The result is presented in Fig. 8. Submonthly variance reduces in $k = 3$ along with the increase in $k = 7, 8$. The change is consistent with the idea of circulation blocking during the extreme heat events on submonthly time scales. These results complement the statistical analysis in previous sections that showed significant energy growth on planetary scales in normalized energy anomalies. The two statistical metrics describe different dynamics, spatial and temporal variance that are coupled through the properties of the mean state (Žagar et al., 2020).

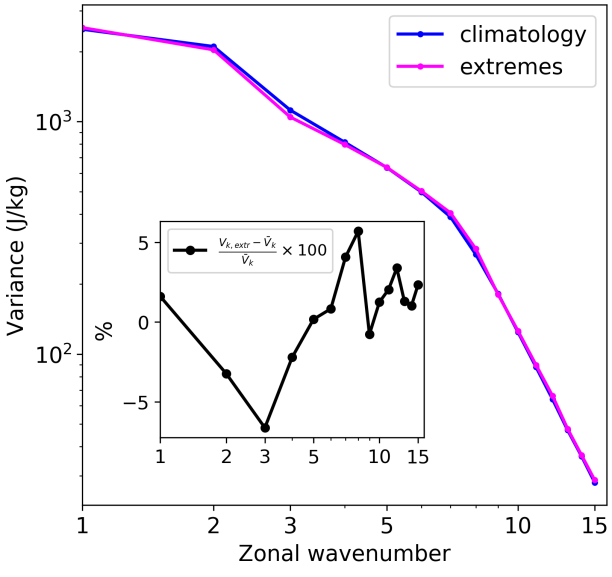


**Figure 8.** Time-averaged submonthly variance spectra of Rossby waves as a function of the zonal wavenumber $k$ with $n = 2-50$ and $m = 1-5$. Averaging is performed over a 40-year period 1980-2019 (blue line) only May-Sep with ERA5 used as input data. The magenta line depicts energy and variance averaged only during heat waves (listed in Table 1). The embedded figures include percentage of relative change.

https://doi.org/10.5194/wcd-2022-23
Preprint. Discussion started: 19 April 2022


Weather and Climate Dynamics Discussions
Open Access
EGU

## 4 Conclusions

Extreme events like heat waves at the surface are accompanied by changes in atmospheric circulation across scales. Our study shows that extremes create a fingerprint in the global circulation. Evidence for the changes in global statistics of the Rossby wave variance is searched in the four modern reanalyses, the ERA5, ERA-Interim, JRA-55, and MERRA datasets. The Rossby waves are identified by a multivariate projection of the global horizontal winds and pseudo-geopotential height on the normal-mode functions on the terrain-following levels. A complete projection basis provides Rossby waves as a function of the zonal wavenumber, meridional mode index and the vertical mode index associated with the vertical structure functions spanning the troposphere and the stratosphere. Scale-selective Rossby wave filtering in physical space is seen as an advantage compared to univariate filtering using the Fourier series along the latitude circles. The reconstructed circulation during heat waves in Eurasia is dominated by the anticyclonic circulation system over northeastern Europe with zonal wavenumbers 2 and 3, which is in agreement with previous studies.

The analysis is carried out on the complex time series of the Hough expansion coefficients representing Rossby modes with the barotropic tropospheric structures. The statistics is performed on the normalized energy anomalies for the total balanced (or Rossby-mode) circulation, for the zonal mean state, and for planetary- and synoptic-scale waves. We show that the single-mode energies follow $\chi^2$-distributions (as sums of squares of independent Gaussian real and imaginary parts). The energy distributions of the zonal mean flow and the planetary circulation are more skewed than other components, with extended right tails. During the surface heat waves, the skewness in planetary waves grows while the opposite occurs in the zonal mean flow, confirming the mechanism of weakening zonal flow and amplification of planetary waves. The symmetric and asymmetric components of the circulation contribute equally to the changes during heat waves over Eurasia.

Our main result is an increase in the skewness of the planetary wave energy anomalies during surface extremes. The increase in skewness can be linked with a decrease in the number of active degrees of freedom in state space during heat waves. A simple estimate based on the $\chi^2$-skewness shows a reduction of the order of $1/4$. This reduction yields a quantitative estimate for the well-known coarse structure of blocking events.

We also discussed changes in time-averaged submonthly variance spectra in the zonal wavenumber domain. We find that the variance decreases for planetary scales and increases for synoptic scales, consistent with the prevalence of atmospheric blocking regime during surface heat waves.

Our analysis of fingerprints of heat waves in the global balanced circulation can be applied to other extreme events as well as to the unbalanced component of the circulation.

*Author contributions.* All authors contributed to the study conception and design. IS developed the algorithm, performed the data analysis and wrote a first draft of the manuscript. All authors participated in data interpretation and revised previous versions of the manuscript. All authors read and approved the final manuscript.

https://doi.org/10.5194/wcd-2022-23
Preprint. Discussion started: 19 April 2022


Weather and Climate Dynamics Discussions
Open Access
EGU

*Competing interests.* The authors declare that the research was conducted in the absence of any commercial or financial relationships that could be construed as a potential conflict of interest.

*Acknowledgements.* This work was funded by the Deutsche Forschungsgemeinschaft (DFG, German Research Foundation) under Germany's Excellence Strategy – EXC 2037 'CLICCS - Climate, Climatic Change, and Society' (CLICCS, A6) – Project Number: 390683824, contribution to the Center for Earth System Research and Sustainability (CEN) of Universität Hamburg. IS thanks Žiga Zaplotnik for the advice on Python and Qiyun Ma for the algorithm for the heat waves identification and discussions.

https://doi.org/10.5194/wcd-2022-23
Preprint. Discussion started: 19 April 2022




## References

Barriopedro, D., Fischer, E. M., Luterbacher, J., Trigo, R. M., and García-Herrera, R.: The Hot Summer of 2010: Redrawing the Temperature Record Map of Europe, Science, 332, 220–224, https://doi.org/10.1126/science.1201224, 2011.

Behera, S. K., Ratnam, J. V., Masumoto, Y., and Yamagata, T.: Origin of extreme summers in Europe: the Indo-Pacific connection, Climate Dynamics, 41, 663–676, 2012.

Coumou, D., Petoukhov, V., Rahmstorf, S., Petri, S., and Schellnhuber, H. J.: Quasi-resonant circulation regimes and hemispheric synchronization of extreme weather in boreal summer, Proceedings of the National Academy of Sciences, 111, 12 331–12 336, https://doi.org/10.1073/pnas.1412797111, 2014.

Coumou, D., Lehmann, J., and Beckmann, J.: Climate change. The weakening summer circulation in the Northern Hemisphere mid-latitudes, Science (New York, N.Y.), 348, https://doi.org/10.1126/science.1261768, 2015.

Dee, D. P., Uppala, S. M., Simmons, A. J., Berrisford, P., Poli, P., Kobayashi, S., Andrae, U., Balmaseda, M. A., Balsamo, G., Bauer, P., Bechtold, P., Beljaars, A. C. M., van de Berg, L., Bidlot, J., Bormann, N., Delsol, C., Dragani, R., Fuentes, M., Geer, A. J., Haimberger, L., Healy, S. B., Hersbach, H., Hólm, E. V., Isaksen, L., Kållberg, P., Köhler, M., Matricardi, M., McNally, A. P., Monge-Sanz, B. M., Morcrette, J.-J., Park, B.-K., Peubey, C., de Rosnay, P., Tavolato, C., Thépaut, J.-N., and Vitart, F.: The ERA-Interim reanalysis: configuration and performance of the data assimilation system, Quarterly Journal of the Royal Meteorological Society, 137, 553–597, https://doi.org/https://doi.org/10.1002/qj.828, 2011.

Fraedrich, K., Ziehmann, C., and Sielmann, F.: Estimates of spatial degrees of freedom, Journal of climate, 8, 361–369, 1995.

Hersbach, H., Bell, B., Berrisford, P., Hirahara, S., Horányi, A., Muñoz-Sabater, J., Nicolas, J., Peubey, C., Radu, R., Schepers, D., et al.: The ERA5 global reanalysis, Quarterly Journal of the Royal Meteorological Society, 146, 1999–2049, 2020.

Kobayashi, S., OTA, Y., HARADA, Y., EBITA, A., MORIYA, M., ONODA, H., ONOGI, K., KAMAHORI, H., KOBAYASHI, C., ENDO, H., MIYAOKA, K., and TAKAHASHI, K.: The JRA-55 Reanalysis: General Specifications and Basic Characteristics, Journal of the Meteorological Society of Japan. Ser. II, 93, 5–48, https://doi.org/10.2151/jmsj.2015-001, 2015.

Kornhuber, K., Osprey, S., Coumou, D., Petri, S., Petoukhov, V., Rahmstorf, S., and Gray, L.: Extreme weather events in early summer 2018 connected by a recurrent hemispheric wave-7 pattern, Environmental Research Letters, 14, 054 002, https://doi.org/10.1088/1748-9326/ab13bf, 2019.

Lau, W. K. M. and Kim, K.-M.: The 2010 Pakistan Flood and Russian Heat Wave: Teleconnection of Hydrometeorological Extremes, Journal of Hydrometeorology, 13, 392 – 403, https://doi.org/10.1175/JHM-D-11-016.1, 2012.

Ma, Q. and Franzke, C. L. E.: The role of transient eddies and diabatic heating in the maintenance of European heat waves: a nonlinear quasi-stationary wave perspective, Climate Dynamics, 56, 2983 – 3002, 2021.

Perron, M. and Sura, P.: Climatology of Non-Gaussian Atmospheric Statistics, Journal of Climate, 26, 1063 – 1083, https://doi.org/10.1175/JCLI-D-11-00504.1, 2013.

Petoukhov, V., Rahmstorf, S., Petri, S., and Schellnhuber, H. J.: Quasiresonant amplification of planetary waves and recent Northern Hemisphere weather extremes, Proceedings of the National Academy of Sciences, 110, 5336–5341, https://doi.org/10.1073/pnas.1222000110, 2013.

Ragone, F. and Bouchet, F.: Rare Event Algorithm Study of Extreme Warm Summers and Heatwaves Over Europe, Geophysical Research Letters, 48, https://doi.org/10.1029/2020gl091197, 2021.

https://doi.org/10.5194/wcd-2022-23
Preprint. Discussion started: 19 April 2022


Rienecker, M. M., Suarez, M. J., Gelaro, R., Todling, R., Bacmeister, J., Liu, E., Bosilovich, M. G., Schubert, S. D., Takacs, L., Kim, G.-K., Bloom, S., Chen, J., Collins, D., Conaty, A., da Silva, A., Gu, W., Joiner, J., Koster, R. D., Lucchesi, R., Molod, A., Owens, T., Pawson, S., Pegion, P., Redder, C. R., Reichle, R., Robertson, F. R., Ruddick, A. G., Sienkiewicz, M., and Woollen, J.: MERRA: NASA's Modern-Era Retrospective Analysis for Research and Applications, Journal of Climate, 24, 3624 – 3648, https://doi.org/10.1175/JCLI-D-11-00015.1, 2011.

Screen, J. A. and Simmonds, I.: Amplified mid-latitude planetary waves favour particular regional weather extremes, Nature Climate Change, 4, 704–709, https://doi.org/10.1038/nclimate2271, 2014.

Sura, P., Newman, M., Penland, C., and Sardeshmukh, P.: Multiplicative Noise and Non-Gaussianity: A Paradigm for Atmospheric Regimes?, Journal of the Atmospheric Sciences, 62, 1391 – 1409, https://doi.org/10.1175/JAS3408.1, 2005.

Teng, H. and Branstator, G.: A Zonal Wavenumber 3 Pattern of Northern Hemisphere Wintertime Planetary Wave Variability at High Latitudes, Journal of Climate, 25, 6756 – 6769, https://doi.org/10.1175/JCLI-D-11-00664.1, 2012.

Teng, H. and Branstator, G.: Amplification of Waveguide Teleconnections in the Boreal Summer, Current Climate Change Reports, 5, 421 – 432, 2019.

Žagar, N. and Tribbia, J.: Modal View of Atmospheric Variability: Applications of Normal-Mode Function Decomposition in Weather and Climate Research, Mathematics of Planet Earth 8, Springer International Publishing;Springer, 1st ed. edn., 2020.

Žagar, N., Kasahara, A., Terasaki, K., Tribbia, J., and Tanaka, H.: Normal-mode function representation of global 3D datasets: open-access software for the atmospheric research community, Geosci. Model Dev., 8, 1169–1195, 2015.

Wiedenmann, J. M., Lupo, A. R., Mokhov, I. I., and Tikhonova, E. A.: The Climatology of Blocking Anticyclones for the Northern and Southern Hemispheres: Block Intensity as a Diagnostic, Journal of Climate, 15, 3459 – 3473, https://doi.org/10.1175/1520-0442(2002)015<3459:TCOBAF>2.0.CO;2, 2002.

Wilks, D. S.: Statistical methods in the atmospheric sciences, vol. 100 of *International Geophysics*, Academic Press, third edn., http://www.sciencedirect.com/science/bookseries/00746142/100/supp/C, 2011.

Xu, P., Wang, L., Liu, Y., Chen, W., and Huang, P.: The record-breaking heat wave of June 2019 in Central Europe, Atmospheric Science Letters, 21, 2020.

Žagar, N., Žiga Zaplotnik, and Karami, K.: Atmospheric Subseasonal Variability and Circulation Regimes: Spectra, Trends, and Uncertainties, Journal of Climate, 33, 9375 – 9390, https://doi.org/10.1175/JCLI-D-20-0225.1, 2020.